Journal of the European Ceramic Society **8** (1991) 365–374

Interrelation among Flaw Resistance, K^R-Curve Behavior and Thermal Shock Strength Degradation in Ceramics. II. Experiment

H. E. Lutz & M. V. Swain

Department of Mechanical Engineering, University of Sydney, Sydney, NSW 2006, Australia

(Received 14 February 1991; revised version received 22 May 1991; accepted 24 May 1991)

Abstract

Indentation-induced flaw resistance, toughness behavior upon crack extension and thermal shock behavior of a range of different ceramics are investigated. The results are analysed and compared with previous theoretical considerations. An attempt is made to establish an interrelation among the above three properties of ceramics.

Für eine Reihe unterschiedlicher keramischer Werkstoffe wurde das R- bzw. K^R-Kurvenverhalten sowie die Thermoschockbeständigkeit untersucht. Die Ergebnisse wurden analysiert und mit früheren theoretischen Überlegungen verglichen. Es wird der Versuch unternommen, zwischen den drei oben erwähnten Eigenschaften von keramischen Werkstoffen einen Zusammenhang abzuleiten.

Nous avons étudié, pour un éventail de céramiques, la résistance à la fissuration induite par indentation, la ténacité par propagation de fissures et le comportement aux chocs thermiques. Les résultats sont analysés en vue d'être confrontés aux considérations théoriques préalables. On essaie notamment d'établir une corrélation entre les trois propriétés pré-citées.

1 Introduction

In the past two decades many new and improved ceramic materials have been developed, opening new fields for the applicability of ceramics. Of particular interest are ceramic refractories which can be used in environments of rapidly changing temperatures. The quality of these materials is generally evaluated by measurements of crack resistance or toughness behavior upon crack extension, namely R- or K^R-curve behavior, and thermal shock properties. However, R- or K^R-curve testing requires both adequate equipment and experience, and, as is thermal shock testing, expensive.

In the accompanying paper[1] an attempt was made to link K^R-curve behavior and thermal shock strength degradation of ceramics with a third more easily measurable property, their flaw resistance. The approach was based on two simplistically formulated relationships, the correlation between flaw resistance and K^R-curve behavior[2] on the one hand and the correlation between the K^R-curve behavior and the thermal shock strength degradation on the other hand.[3–9]

Cook & Clarke[2] suggested that the relationship between the indentation-induced flaw resistance and the steepness of the K^R-curve can be quantitatively described by

$$\log\left[\frac{\sigma_I^2}{\sigma_I^1}\right] = \left(\frac{2\tau - 1}{2\tau + 3}\right) \log\left[\frac{P_I^2}{P_I^1}\right] \qquad (1)$$

where σ_I^2 and σ_I^1 are the anticipated values of the retained strength after damaging the surface of a material by Vickers indentations of loads P_I^2 and P_I^1, respectively, and τ is the logarithmic slope of the K^R-curve of the material. A plot of $\log \sigma_I$ versus $\log P_I$ is expected to result in a straight line with slope $(2\tau - 1)/(2\tau + 3)$. This slope is an indicator of the flaw resistance of the material. Since it contains τ it depends on the steepness of the K^R-curve. For $\tau = 0$ (flat K^R-curve) the absolute value of the slope is a maximum with $\frac{1}{3}$, indicating that the material is 'ideal flaw-sensitive'. With increasing τ (increasingly pronounced K^R-curve behavior) the absolute value of the slope decreases approaching 0 at $\tau = 0{\cdot}5$, indicating 'ideal flaw tolerance'.

The correlation between the K^R-curve behavior and the thermal shock retained strength is neither

Journal of the European Ceramic Society 0955-2219/91/$3.50

described satisfactorily by the empirical Hasselman thermoelastic approach[3,4] nor by the more sophisticated K approach from Evans & Charles.[8] In the accompanying paper[1] a rather simplistic approach was made to derive a relationship between τ and the thermal shock retained strength based on considerations made by Hasselman[3,4] and Homeny and Bradt.[5] Assuming that the material behaves linear elastically and that the temperature does not influence the R-curve behavior of the material, and hence the value of τ, the correlation between the thermal shock retained strength, σ_R, when related to the initial strength, σ_B, and τ can be described by[1]

$$\frac{\sigma_R}{\sigma_B} = \frac{2{\cdot}25}{(1+\tau)^2}\left(\frac{a}{a_0}\right)^{(2\tau-1)} \quad (2)$$

where a is the crack length and a_0 the spatial extent of the crack at which toughening begins.

The aim of the accompanying paper[1] was to compare the relationship between the flaw resistance and the K^R-curve slope τ described by eqn (1) with the correlation between τ and the thermal shock strength degradation described by eqn (2). Assuming that both correlations are valid the retained strength of a ceramic after mechanically introduced surface damage and after a severe thermal shock event show surprising similarities in their dependence on τ. If it would be possible to establish an empirical interrelation among all three properties, flaw resistance, K^R-curve behavior and thermal shock strength degradation, two of them could be easily predicted by the knowledge of one alone.

The aim of this work is to investigate and compare flaw resistance, K^R-curve behavior and thermal shock behavior of different ceramic materials. For a comparison of the results an attempt will be made to use τ as a quantitative measure for flaw resistance and K^R-curve behavior of the tested materials. The results are discussed with respect to the theoretical considerations in the accompanying paper.[1]

2 Experimental Procedure

The tests were carried out on the following materials.

(1) Si_3N_4 composites containing 10, 20, 30 and 40 wt% BN (Kawasaki Steel, Japan). Fabrication conditions, microstructure and mechanical properties of these materials are described in detail by Isomura *et al.*[10] The composites, Si_3N_4 + 10, 20, 30 and 40 vol.% BN, are labeled SNB10, SNB20, SNB30 and SNB40, respectively.

(2) Al_2O_3 with grain size of ~1 μm, 2Y-TZP, 3Y-TZP + 20 wt% Al_2O_3, and various duplex-ceramics (composites AB) having these materials as matrix (component A). Different mixtures of Al_2O_3 (CT 8000 SG, Alcoa) and 35, 50, 80 vol.% m-ZrO_2 (Dynazirkon F, Dynamit Nobel) and pure m-ZrO_2 were used as inclusion component B. The materials were sintered at 1500°C for 2 h and, in some instances, hot isostatically pressed (HIPed) at 200 MPa at 1600°C for 10 min in N_2. The fabrication procedure of these composites is described in detail by Lutz & Claussen.[11]

For further discussions the matrix components (A), 2Y-TZP, 3Y-TZP + 20 wt% Al_2O_3 and Al_2O_3, are labeled 2YZ, 3YZ20A and AO, respectively. The pressure zone components (B), Al_2O_3 + 35, 50 vol.% m-ZrO_2 and pure m-ZrO_2, are labeled az35, az50 and z100, respectively. For small (16–32 μm diameter) and large (45–65 μm diameter) pressure zones the indexes 'S' and 'L' are used, respectively. The duplex-ceramic labeled 3YZ20A-20az50$_S$, for example, consists of 20 vol.% of small pressure zones composed of Al_2O_3 + 50 vol.% m-ZrO_2 dispersed within a matrix 3Y-TZP + 20 wt% Al_2O_3.

(3) Precipitated partially stabilized zirconia containing 9 mole% MgO (i.e. Mg-PSZ). Simultaneous sintering and heat treatment in the cubic phase field, followed by controlled cooling and subeutectoid heat treatment for longer periods, resulted in materials of maximum strength (MS) and high thermal shock resistance (TS).[12] The fabrication heat treatment and resultant microstructures have been described in detail by Hannink[13] and Hannink & Swain.[14]

The flaw resistance tests were carried out on small rectangular beams (for dimensions see below) using the indentation strength in bending (ISB) method.[15] The specimens had the following dimensions: SNB materials: 5·2–6·2 × 2·5–3·1 × 32 mm: Al_2O_3, 2YZ, 3YZ20A and duplex-ceramics based on these materials: 2·9–3·4 × 3·2–3·8 × 45 mm; Mg-PSZ (MS and TS): 3·4 × 4·4–4·8 × 42 mm. The smaller side of the specimens was indented using various loads between 1 and 1000 N. The retained strength was measured in four-point bending (span 18/6 mm) with a cross-head speed of 0·3 mm/min.

The K^R-curve experiments were performed using compact tension (CT) tests. One side of the testpieces was polished. The samples were precracked by starting the crack from a chevron-like prenotch. When a sharp straight-through crack was achieved the specimens were renotched to a point as near as possible behind the crack front. The notch depth/sample width ratio, a_0/w, was chosen to be 0·51–0·61 for the SNB specimens and 0·58–0·65 for all other materials. The samples were loaded using a cross-

head speed of 10 μm/min. The crack propagation was measured directly using a traveling microscope. The K^R-values were calculated on the basis of the load P, the relative crack length a/w, the sample thickness b and the appropriate Y-function, namely[16]

$$K^R = Y(a/w)\frac{P}{bw^{1/2}} \tag{3}$$

for $a/w \leq 0{\cdot}85$ with

$$Y(a/w) = \frac{(2+a/w)}{(1-a/w)^{3/2}} \times [0{\cdot}886 + 4{\cdot}64(a/w) - 13{\cdot}32(a/w)^2 + 14{\cdot}72(a/w)^3 - 5{\cdot}6(a/w)^4] \tag{4}$$

The CT samples had the following dimensions: SNB materials: 25–27 × 32 × 5·2–6·2 mm; Al_2O_3, 2YZ, 3YZ20A and duplex-ceramics based on 2YZ and 3YZ20A: 21–22 × 26–27 × 2·9–3·4 mm.

Based on the assumption that the flaw resistance of the ISB-tested materials obey eqn (1) suggested by Cook & Clarke,[2] with the slope of the resulting $\log(\sigma_R)/\log(P_1)$ plots being $(2\tau-1)/(2\tau+3)$, 'τ_{ISB}' was calculated from the slope obtained by a linear regression of all measured data points. For a direct comparison with the K^R-curves the logarithmic steepness, 'τ_K', of the measured K^R-curves was evaluated in a similar procedure, namely by linear regression of the $\log(K^R)/\log(a)$ plots.

Thermal shock tests were carried out by measuring the retained bending strength after quenching samples from successively higher temperatures into 20°C water. Their strength or modulus of rupture (MOR) was measured in four-point bending (span 24/8 and 18/6 mm) at a cross-head speed of 0·3 mm/min. The specimens had the following dimensions: SNB materials: same as for ISB testing; Al_2O_3, 2YZ, 3YZ20A and duplex-ceramics based on these materials: 3·5 × 3·5 × 45 mm.

3 Results

The results of the ISB tests, K^R-curve measurements and thermal shock tests are shown in detail in Figs 1–4. The results also include numerous other data published by different authors[9,10,12,17–21] in the last few years.

Figure 1 contains results obtained from different grain-sized (1–16 μm) aluminas. The top diagram shows the indentation-induced flaw resistance curves measured by Chantikul *et al.*[18] for 2·5 and 14·6 μm alumina using Vickers indentation loads of

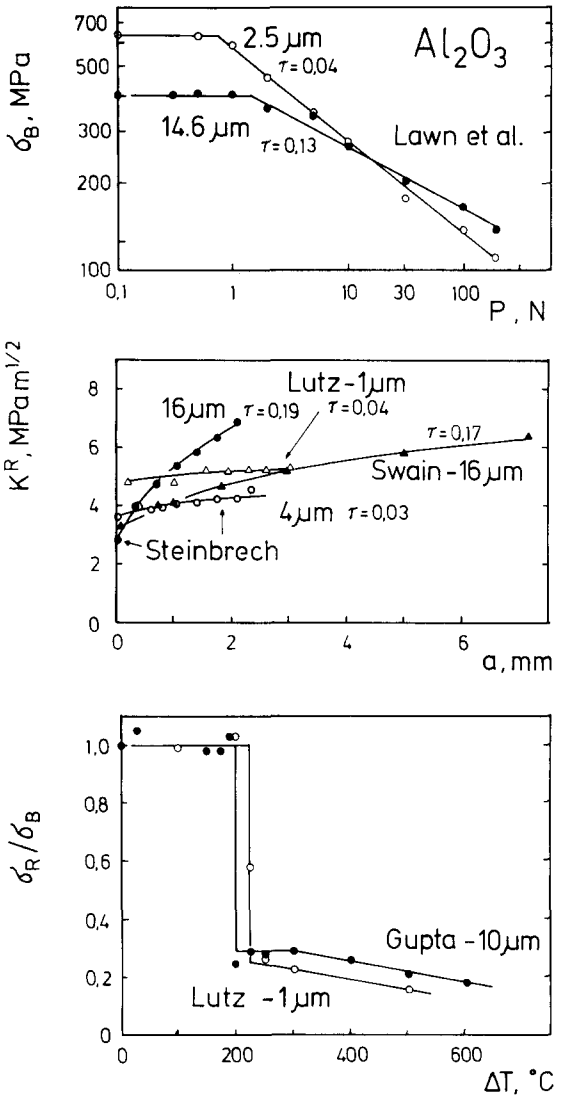

Fig. 1. Flaw resistance (top), K^R-curve behavior (middle) and thermal shock behavior (bottom) of alumina ceramics of different grain size.

0·3–200 N. Although the finer grain-sized aluminas exhibit higher initial strength the material is more flaw-sensitive, showing a steeper decrease in retained strength with increasing Vickers indentation load than the coarser grain-sized alumina. The diagram in the middle illustrates the K^R-curve behavior of 1 μm alumina compared to curves borrowed from Steinbrech *et al.*[19] and Swain.[20] Two curves for 4 and 16 μm materials have been calculated from the R-curves measured by Steinbrech[19] in three-point bending (SENB specimen dimensions 7·0 × 5·0 × 60 mm). Another curve has been obtained from a DCB test (specimen dimensions 3·3 × 14·2 × 80 mm) performed by Swain,[20] with the 16 μm alumina fabricated by Steinbrech. The K^R-curve behavior of the 1 and 4 μm materials are very similar and almost flat. Although the curves reported by Steinbrech *et al.*[19] and Swain[20] for exactly the same 16 μm alumina are different as a result of the different

sample geometry and testing technique, they show a similar steepness τ with 0·19 and 0·17.

The thermal shock behavior of 1 and 10 μm materials is demonstrated in the lower diagram in the form of the normalized retained strength, σ_R/σ_B, versus the quenching temperature difference, ΔT. The curve of the 10 μm material has been borrowed from Gupta.[21] This material shows a slightly reduced ΔT_c when compared to the 1 μm alumina, but also slightly higher retained strength after severe thermal shocks.

Flaw resistance, K^R-curve behavior and thermal shock behavior of the two Mg-PSZ ceramics are depicted in Fig. 2 and compared with curves of HIPed 2YZ and the 2YZ-based duplex-ceramic, 2YZ-10az35$_L$. The K^R-curve and thermal shock behavior of the MS and TS Mg-PSZ materials were published by Marshall & Swain[12] and Hannink & Swain[14] in previous papers. There is no significant difference in the flaw resistance of the two differently aged ceramics although their K^R-curve and thermal shock behavior are different. The incorporation of pressure zones in 2YS leads to a pronounced strength reduction, but also to an increased flaw resistance, steeper K^R-curve and higher thermal shock retained strength.

The tremendous change in the mechanical and thermal shock properties of a brittle high-strength matrix which can be achieved by incorporating pressure zones is demonstrated in Fig. 3 for the matrix 3YZ20A. As has been previously illustrated,[11,22–25] and as is here apparent from Fig. 3, the strength of the matrix decreases increasingly with 20 vol.% of small az50 zones, and 10 and 20 vol.% of small z100 zones, i.e. with increasing amounts and volume expansion of the zones, whereas the resistance to mechanically introduced surface flaws and severe thermal shocks and the steepness of the K^R-curves increase. Another interesting feature of the K^R-curve behavior of

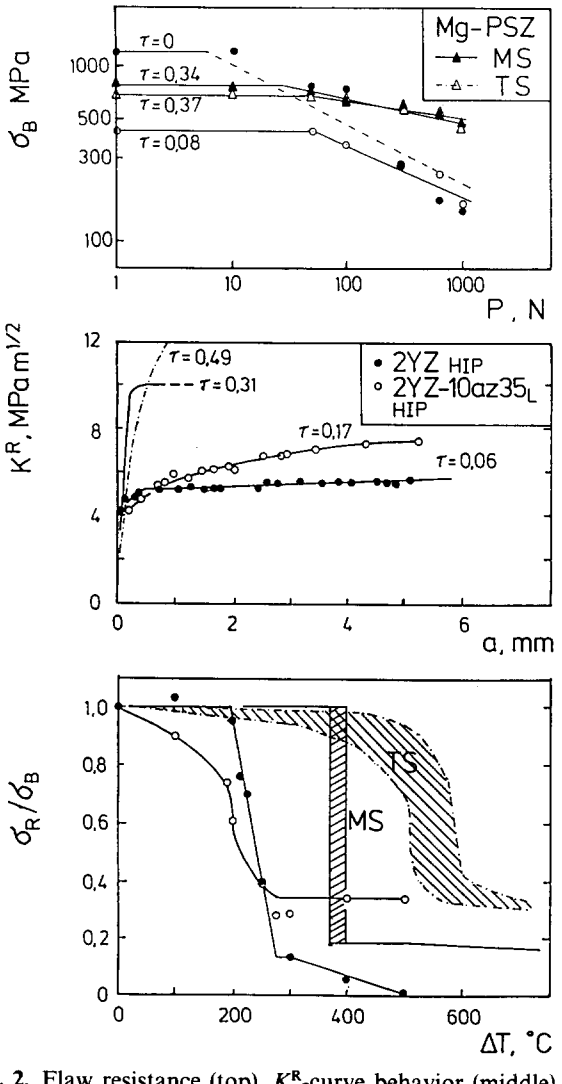

Fig. 2. Flaw resistance (top), K^R-curve behavior (middle) and thermal shock behavior (bottom) of two differently aged Mg-PSZ ceramics, 2Y-TZP (2YZ) and 2YZ-10az35$_L$.

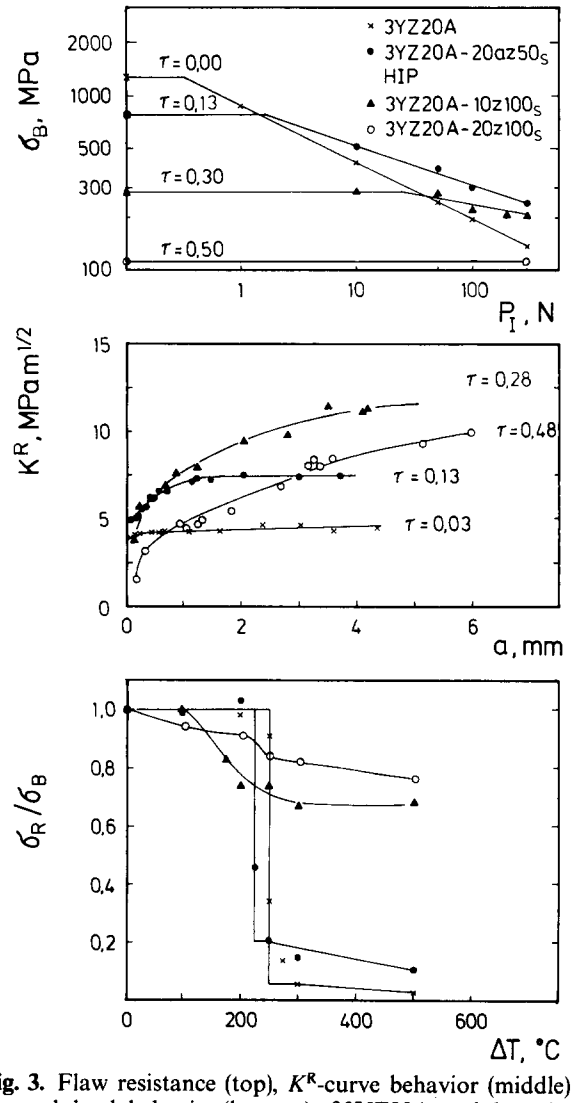

Fig. 3. Flaw resistance (top), K^R-curve behavior (middle) and thermal shock behavior (bottom) of 3YZ20A, and three duplex-ceramics, 3YZ20A-20az50$_S$, -10z100$_S$ and -20z100$_S$.

duplex-ceramics is that although its steepness increases the location of the curves is first shifted to higher K^R-values, passes through a maximum and decreases again. This effect can be observed in Fig. 3 by comparing the curve of 3YZ20A-10z100$_S$ exhibiting a τ-value of only 0·28 with the curve of 3YZ20A-20z100$_S$, which shows a logarithmic slope as high as 0·48. The K^R-values of 3YZ20A-20z100$_S$ are on average lower but describe a steeper (logarithmic) path than the curve of 3YZ20A-10z100$_S$.

Flaw resistance, K^R-curve behavior and thermal shock behavior of the SNB materials are shown in Fig. 4.[26] The thermal shock results have been borrowed from a paper of Isomura *et al.*,[10] with the exception of the result for $\Delta T = 1200°C$. All materials show similar flaw resistance behavior. The strength reduction is quite low for indentation loads

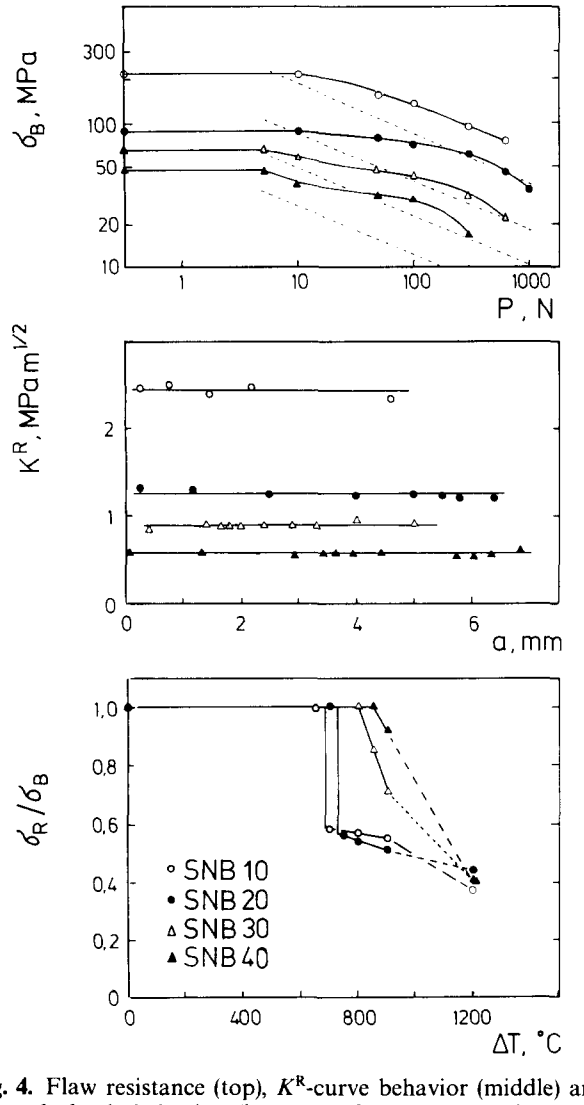

Fig. 4. Flaw resistance (top), K^R-curve behavior (middle) and thermal shock behavior (bottom) of SNB composites. The broken lines (top) are the anticipated response of the various SNB materials using the K^R-curve plateau values as K_{Ic} for the calculation of the ISB retained strength.[26] The basis for the overestimation of K_{Ic} by using the ISB technique is discussed in the text.

up to 100 N but is apparently more pronounced for higher loads, with a final slope of the curves closer to (−1/3). All SNB composites exhibit flat K^R-curves with their toughness decreasing with increasing BN content. A thermal shock of $\Delta T = 1200°C$ into water at room temperature results in a strength loss of 56–66%. The retained strength of the SNB ceramics subjected to such severe thermal shock decline in proportion to their initial strength as the BN content increases.

4 Discussion

A comparison of the resulting flaw resistance, K^R-curve and thermal shock behavior show that there are clear trends in the interrelation among all three properties. These trends are not only found in alumina and Mg-PSZ but also in complex duplex structures and to some extent in Si_3N_4 BN structures exhibiting residual porosity. As has been pointed out in the accompanying paper,[1] there are countless parameters which can influence the experimental results which are thought to be responsible for certain limitations in the quantitative applicability of this interrelation. Major limitations seem to come from the restricted applicability of the ISB method for determining the flaw resistance, especially in porous and quasi-ductile materials, and the unknown influence of temperature and quasi-plasticity on the material's behavior during thermal shock.

There is also some doubt concerning the characterization of the flaw resistance by a measure of τ because this assumes that the logarithmic decrease of the strength with increasing Vickers indentation load obeys a linear relationship. Most ceramics, however, show a deviation from linearity for certain indentation loads, an effect which can be caused, for example, by a load-dependent change of the crack pattern beneath the indentation.[27] Localized residual compressive stresses which can develop about the indentation due to stress-induced transformation in zirconia-containing ceramics are reported to reduce the initial crack length[28] and counteract crack propagation upon applied stress for low indentation loads. At higher indentation loads, on the other hand, the cracks can overpass the transformation zone and extend into the surrounding tensile zone.[29] As a direct consequence a much lower applied stress is required to lead to further propagation and fracture. This may explain the enormous deviation of the flaw resistance curve from linearity (dotted line in Fig. 2(a)) observed in 2Y-TZP. Up to about 100 N indentation load the

damage caused by the indentation does not have a considerable influence on the strength of the material, a situation which abruptly changes for indentation loads of 300 N and more. This behavior is not observed in Mg-PSZ, but may occur in these materials at high loads exceeding 600 N. Most likely, many other effects, in addition to the R-curve behavior, can lead to a steadily changing decline of the strength with increasing indentation load.

Of particular interest here is to study the difference between τ_{ISB} calculated from the resulting flaw-resistance line and the retained strength after a Vickers indentation of a certain load, σ_R, when normalized to the initial strength, σ_B. It is expected that the relationship between σ_R/σ_B and τ_{ISB} is different from the relationship in eqn (1). This is because eqn (1) only considers the strength reduction in the indentation load region where strength degradation occurs, whereas σ_R/σ_B also takes the region of constant strength at small indentation loads into account. This plateau region differs from material to material. In general, it seems to increase with increasing flaw tolerance. In Fig. 5 σ_R/σ_B obtained after a 30-kg Vickers indentation is plotted versus τ_{ISB}. The plot reveals a nearly linear relationship indicated by the dotted line. The (σ_I^2/σ_I^1) values calculated from eqn (1) for $(P_I^2/P_I^1) = 50$ are shown as the solid curve in Fig. 5. Both curves are similar for flaw-tolerant materials, but show an increasing divergence for flaw-sensitive materials (small τ_{ISB} values). The reason is that the considered strength degradation range of the flaw-tolerant materials is comparable to the (P_I^2/P_I^1) ratio of 50, which has been chosen here for comparison. In the flaw-sensitive composites, however, the strength degradation region already starts at relatively small indentation loads ($\leq$1 N) and is hence, with c. 1–300 N, larger than in the flaw-tolerant materials. The larger the strength degradation region, i.e. the (P_I^2/P_I^1) ratio, the smaller is the resulting (σ_I^2/σ_I^1) value according to eqn (1). It is, nevertheless, surprising that the plot of (σ_R/σ_B) versus τ_{ISB} gives an almost linear trend despite the exponential relationship between (σ_I^2/σ_I^1) and τ_{ISB} in eqn (1).

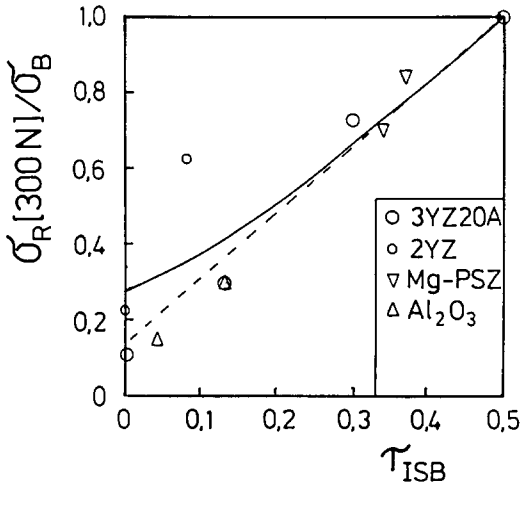

Fig. 5. Plot of the normalized retained strength, σ_R/σ_B, of MS and TS grade (Mg-PSZ), Al_2O_3 of different grain size, and different duplex-ceramics with matrices 3YZ20A and 2YZ, after a 30-kg Vickers indentation versus τ_{ISB}, calculated from the logarithmic slope of their flaw-resistance curves. The linear arrangement of the points shown by the dotted line is similar to the solid curve calculated from eqn (1) for $(P_I^2/P_I^1) = 50$.

A good interrelationship between flaw resistance and K^R-curve behavior is found in groups of related materials. This is apparent from the plot of the τ_{ISB} versus the τ_K values in Fig. 6, which confirms eqn (1) suggested by Cook & Clarke.[2] The enormous deviation for the TS grade from the general trend is due to the fact that its flaw resistance is much lower than anticipated from its extremely pronounced K^R-curve behavior. The pronounced quasi-ductility of Mg-PSZ seems to represent a major problem for the applicability of the ISB technique and reliability of the results. Vickers indentations of up to 100 N lead to no cracking, indentations of higher load to an 'ill-defined' crack pattern. Besides lateral cracks causing chipping around the indentation, 8–12 short cracks develop radially around the Vickers indentation instead of the four anticipated cracks starting from the indentation corners. The length of these cracks lies in the range of a half indentation diameter.

The plot of the normalized retained strength, σ_R/σ_B, after a thermal shock of $\Delta T = 500°C$ versus τ_{ISB} and τ_K in Fig. 7 reveals the relationship between the retained strength and τ. The trend is illustrated by the dotted line. The retained strength increases first linearly with increasing τ and seems to approach a constant value of c. 0·8 with τ exceeding 0·3. This is

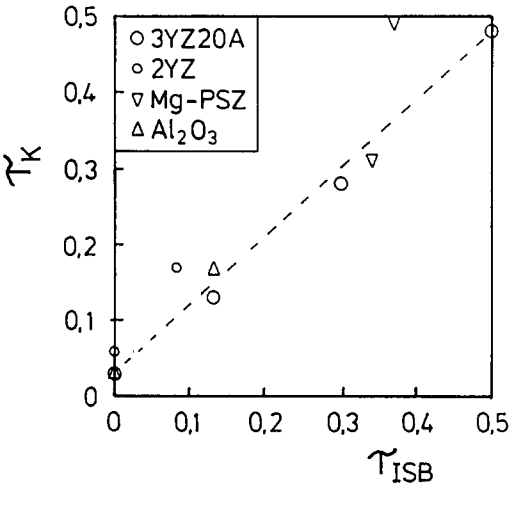

Fig. 6. Plot of the logarithmic slope of the K^R-curves, τ_K, of all tested materials versus τ_{ISB}.

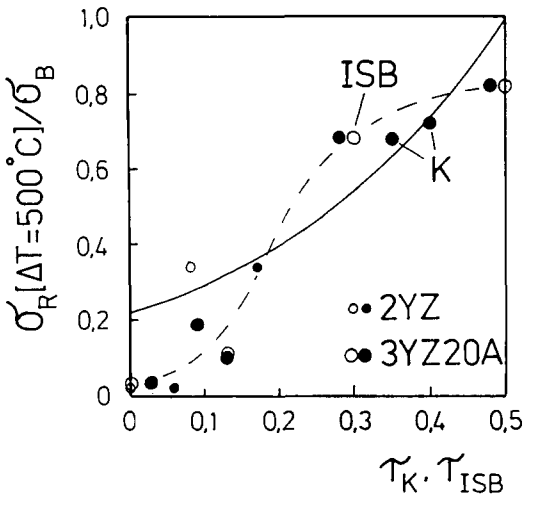

Fig. 7. Plot of the normalized retained strength, σ_R/σ_B, after a thermal shock of $\Delta T = 500°C$ versus τ_{ISB} and τ_K for 2YZ, 3YZ20A and various duplex-ceramics with these matrices. The main tendency given by the dotted line is compared with eqn (2) calculated for $(a/a_0) = 10$ and shown as a solid line.

different from the curving behavior predicted by eqn (2) calculated for $(a/a_0) = 10$ and shown as a solid line in Fig. 7. It seems that the lack of knowledge about the role of temperature and quasi-plasticity during thermal stress fracture is the main reason for the unsatisfactory predictability of the retained strength.

The thermal shock retained strength can also be compared directly with the ISB retained strength. In Fig. 8 the normalized retained strength after a 30-kg indentation of a wide range of differently composed

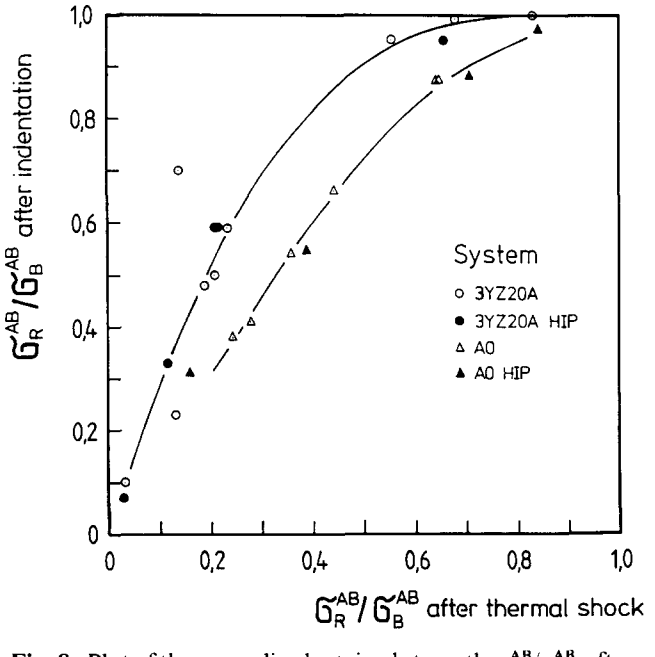

Fig. 8. Plot of the normalized retained strength, $\sigma_R^{AB}/\sigma_B^{AB}$, after a 30-kg indentation of a wide range of differently composed duplex-ceramics (composites AB) with matrices AO and 3YZ20A versus their normalized retained strength after a thermal shock of 500°C.

duplex-ceramics with matrices AO and 3YZ20A is plotted versus their normalized retained strength after a thermal shock of 500°C. The data of the AO-based duplex-ceramics show a more linear fit and a shift to higher thermal shock retained strength. This is thought to be due to the high temperature sensitivity of the 3Y-TZP-containing matrix.[30] The reduced transformability of ZrO_2 in all ZrO_2 ceramics is their main disadvantage and has a pronounced effect on their thermal shock behavior. This becomes obvious for Mg-PSZ and 2Y-TZP ceramics, which show a considerably high thermal shock strength degradation despite their pronounced *R*-curve behavior.

In recent papers[11,22–25,31] the so-called 'internal stress-intensity factor K_i' has been suggested as a measure by which duplex-ceramics can be successfully classified. If ε^v is the effective volume expansion of the incorporated pressure zones, V_f the volume fraction of zones in the matrix and R_B their mean radius

$$K_i \sim \varepsilon^v(1 + 2{\cdot}7V_f)R_B^{1/2} \tag{5}$$

and hence increases with increasing amount, size and volume expansion of the zones. K_i is a measure of the

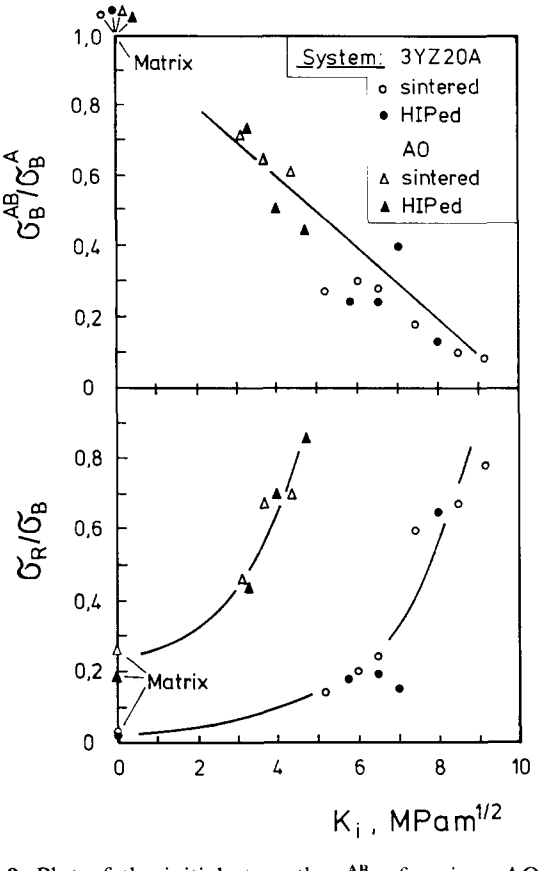

Fig. 9. Plot of the initial strength, σ_B^{AB}, of various AO- and 3YZ20A-based duplex-ceramics where related to the respective value of their pure matrix, σ_B^A, and their normalized retained strength, σ_R/σ_B, after a thermal shock of $\Delta T = 500°C$ versus the internal stress-intensity factor, K_i.

propensity of the internal stresses to manifest fracture or assist in the nucleation of cracks with the application of external stresses.

For the duplex-ceramics 3YZ20A-20az50$_S$, -10z100$_S$ and -20z100$_S$ K_i is 5·8, 7·1 and 8·6 MPa m$^{1/2}$, respectively. Of particular interest here is to compare the results for the duplex-ceramics also with the measure K_i. Figure 9 shows that the initial strength of duplex-ceramics, σ_B^{AB}, when related to the respective value of their pure matrix, σ_B^A, continuously decreases by incorporating pressure zones of increasing K_i.[22] In contrast to the tendency in the initial strength, the normalized thermal shock retained strength of duplex-ceramics rises continuously with increasing K_i, showing first a slight increase followed by a steep rise for higher K_i-values.[23] The relation of the thermal shock retained strength versus K_i for the two different duplex systems leads to two different curves. This is thought to be due to the fact that K_{Ic} of the matrix 3YZ20A is comparable to K_{Ic} of AO at room temperature, but is greatly reduced at higher temperatures compared to AO due to the reduced transformability of 3Y-TZP.

The plot of K_i versus τ_{ISB} and τ_K is illustrated in Fig. 10. In addition to the three 3YZ20A-based duplex-ceramics tested here, values of τ_K, σ_R/σ_B after a thermal shock of $\Delta T = 500°C$ and K_i obtained from three other 3YZ20A-based materials published elsewhere,[32] 3YZ20A-20az35$_S$ ($\tau_K = 0{\cdot}09$; $K_i = 3{\cdot}9$ MPa m$^{1/2}$), -20az80$_S$ ($\tau_K = 0{\cdot}35$; $K_i = 7{\cdot}3$ MPa m$^{1/2}$) and -10az80$_L$ ($\tau_K = 0{\cdot}40$; $K_i = 9{\cdot}1$ MPa m$^{1/2}$), are also shown in Figs 7 and 10. For low K_i, τ is only slightly enhanced, indicating that the incorporation of low-volume fractions of small and weak pressure zones do not improve flaw resistance and K^R behavior considerably. At about $K_i = 6$–7 MPa m$^{1/2}$, however, τ rises steeply, showing the tremendous effect of strong pressure zones surrounded by long-ranging stress domains.

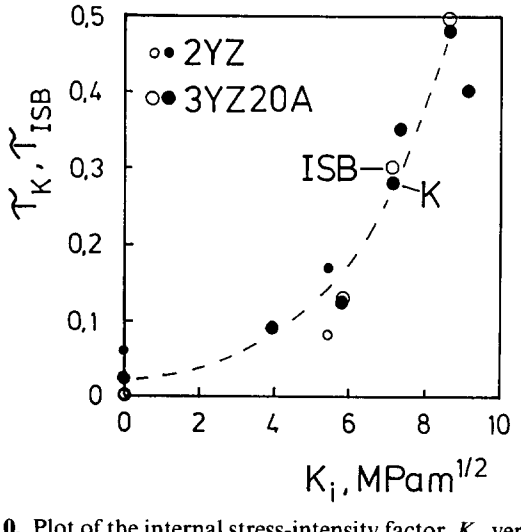

Fig. 10. Plot of the internal stress-intensity factor, K_i, versus τ_K and τ_{ISB} for 2YZ, 3YZ20A and various duplex-ceramics with these matrices.

The flaw-resistance behavior of the SNB composites could be interpreted as indicating *R*-curve behavior. The K^R tests, however, reveal that all SNB composites exhibit flat K^R-curves. The flat K^R-curve behavior which is unaffected by increased BN contents also explains the severe thermal shock strength degradation which is similar in all SNB mixtures. Assuming that the measured plateau values represent K_{Ic} of these obviously brittle materials,[26] it is possible to reconstruct the flaw-resistance curves anticipated from the K^R results using the expression to calculate the ISB toughness.[15] The resulting lines which consequently exhibit the logarithmic slope of $(-1/3)$ ($\tau_{ISB} = 0$) are shown in Fig. 4 as broken lines. It is apparent that the ISB results greatly overestimate the measured K^R-values. A possible explanation for this significant difference may be the reduction in residual stresses about the indentation impression due to the intrinsic porosity of these pressureless sintered materials. For the failure of a brittle material from a mechanically introduced flaw of size c under uniform applied stress σ_a the net stress-intensity factor is considered to be the sum of K_a and K_r, the components for uniform applied stress and for localized loading, namely

$$K = \chi P_l / c^{3/2} + \psi \sigma_a c^{1/2} \tag{6}$$

χ is a numerical constant depending on the contact geometry and the elastic/plastic properties of the material, and ψ is a numerical crack geometry parameter (e.g. $\pi^{1/2}$ for an embedded linear crack and $2/\pi^{1/2}$ for an embedded circular crack).

Upon indentation the region beneath the contact area would be expected to densify. SEM observations showed that no well-defined radial cracks developed from the corners of the impression, rather the size of the cracks only extends slightly beyond the densified region, from which the sample fractures.[26] Assuming that the crack length equals half of the impression diameter, which is *c.* 1·0 mm for a 1000-N indentation in SNB 20, the calculation of K_{Ic} using only the component K_a in eqn (2) with $\psi = 2/\pi^{1/2}$ gives exactly the K^R-value of 1·2 MPa m$^{1/2}$. This may indicate that the contribution of K_r to K_{Ic} can almost be neglected in these materials.

The present study suggests that there are limitations to the approach outlined in the accompanying paper,[1] particularly for transformation-based quasi-ductile materials such as Mg-PSZ and the fine-grained porous Si_3N_4-BN composites. In

both instances the concept breaks down because the ISB technique appears unsuitable for the determination of the *R*-curve behavior.

5 Conclusions

Investigations of flaw resistance, K^R-curve and thermal shock behavior of different ceramics show that there is a clear qualitative, but only semi-quantitative, interrelation among all three properties. The results confirm the relationship between flaw resistance and K^R-curve behavior suggested by Cook & Clarke. The experimentally found correlation between the thermal shock retained strength and the steepness of the K^R-curve, however, differs from the theoretically predicted relationship. It is found that the logarithmic slopes of flaw resistance and K^R-curves represent easily evaluated and useful measures for their characterization and for the prediction of the strength degradation upon severe thermal shocks. These measures, however, cannot be used unreservedly. For ductile-behaving materials and porous ceramics the ISB-derived flaw resistance is not suitable for the prediction of *R*-curve behavior and thermal shock strength degradation.

Acknowledgements

One of the authors (H.E.L.) thanks the Deutsche Forschungsgemeinschaft, Bonn, West Germany, for financial support under contract number lu 416/1-1. N. Claussen and P. Greil are thanked for their assistance to make this project possible.

References

1. Lutz, H. E. & Swain, M. V., Interrelation among flaw resistance, K^R-curve behavior and thermal shock strength degradation in ceramics—I. Theoretical considerations. *J. Europ. Ceram. Soc.*, **8** (1991) 355–63.
2. Cook, R. F. & Clarke, D. R., Fracture stability, *R*-curves and strength variability. *Acta Met.*, **36**(3) (1988) 555–62.
3. Hasselman, D. P. H., Unified theory of fracture initiation and crack propagation in brittle ceramics. *J. Am. Ceram. Soc.*, **52**(11) (1969) 600–4.
4. Hasselman, D. P. H., Severe thermal environments figures of merit for thermal shock resistance of high temperature brittle materials. *Ceramurgia Int.*, **4** (1978) 147–51.
5. Homeny, J. & Bradt, R. C., Thermal shock of refractories. In *Thermal Stresses in Severe Environments*, ed. D. P. H. Hasselman & R. A. Heller. Plenum Press, New York, 1980, pp. 343–63.
6. Swain, M. V., *R*-curve behavior of magnesia–partially stabilized zirconia and its significance to thermal shock. In *Fracture Mechanics of Ceramics, Vol. 6*, ed. R. C. Bradt, A. G. Evans, D. P. H. Hasselman & F. F. Lange. Plenum Press, New York, 1983, pp. 345–59.
7. Evans, A. G., Thermal fracture in ceramic materials. *Proc. Brit. Ceram. Soc.*, **25** (1975) 217–35.
8. Evans, A. G. & Charles, E. A., Structural integrity in severe thermal environments. *J. Am. Ceram. Soc.*, **60**(1–2) (1977) 22–8.
9. Swain, M. V., *R*-curve behavior and thermal shock resistance of ceramics. *J. Am. Ceram. Soc.*, **73**(3) (1990) 621–8.
10. Isomura, K., Fukuda, T., Ogasahara, K., Funahashi, T. & Uchimura, R., Machinable Si_3N_4-BN composite ceramics with high thermal shock resistance, high erosion resistance. Anaheim, American Refractory Meeting, The American Ceramic Society.
11. Lutz, H. E. & Claussen, N., Duplex-ceramics. I: Stress calculations, fabrication, and microstructure. *J. Europ. Ceram. Soc.*, **7** (1991) 209–18.
12. Marshall, D. B. & Swain, M. V., Crack resistance curves in magnesia–partially stabilized zirconia. *J. Am. Ceram. Soc.*, **71**(6) (1988) 399–407.
13. Hannink, R. H. J., Microstructural development of subeutectoid-aged zirconia alloys. *J. Mater. Sci.*, **18**(2) (1983) 457–70.
14. Hannink, R. H. J. & Swain, M. V., Magnesia–partially stabilized zirconia: the influence of heat treatment on thermomechanical properties. *J. Austr. Ceram. Soc.*, **18**(2) (1982) 53–62.
15. Chantikul, P., Anstis, G. R., Lawn, B. R. & Marshall, D. B., A critical evaluation of indentation techniques for measuring fracture toughness. II: Strength method. *J. Am. Ceram. Soc.*, **14**(9) (1981) 539–43.
16. *ASTM Standard E399-81.* Annual Book of ASTM Standards, Part 10, 1981.
17. Swain, M. V., *R*-curve behavior of magnesia–partially stabilized zirconia and its significance to thermal shock. In *Fracture Mechanics of Ceramics, Vol. 6*, ed. R. C. Bradt, A. G. Evans, D. P. H. Hasselman & F. F. Lange. Plenum Press, New York, 1983, pp. 345–59.
18. Chantikul, P., Bennison, S. J. & Lawn, B. R., Role of grain size in the strength and *R*-curve properties of alumina. *J. Am. Ceram. Soc.*, **73**(8) (1990) 2419–27.
19. Steinbrech, R., Reichl, A. & Schaarwaechter, W., *R*-curve behaviour of long cracks in alumina. *J. Am. Ceram. Soc.*, **73**(7) (1990) 2009–15.
20. Swain, M. V., *R*-curve behaviour in a polycrystalline alumina material. *J. Mater. Sci. Lett.*, **5** (1986) 1313–15.
21. Gupta, T. K., Strength degradation and crack propagation and thermally shocked Al_2O_3. *J. Am. Ceram. Soc.*, **55** (1972) 249–53.
22. Lutz, H. E. & Claussen, N., Duplex-ceramics. II: Strength and toughness. *J. Europ. Ceram. Soc.*, **7** (1991) 219–26.
23. Lutz, H. E., Claussen, N. & Swain, M. V., K^R-curve behavior of duplex-ceramics. *J. Am. Ceram. Soc.*, **74**(1) (1991) 11–18.
24. Lutz, H. E., Swain, M. V. & Claussen, N., Thermal shock behavior of duplex-ceramics. *J. Am. Ceram. Soc.*, **74**(19) (1991) 19–24.
25. Lutz, H. E. & Swain, M. V., Mechanical and thermal shock properties of duplex-ceramics. *Materials Forum*, **15** (1991) in press.
26. Lutz, H. E. & Swain, M. V., Fracture toughness and thermal shock behavior of silicon nitride–boron nitride ceramics. *J. Am. Ceram. Soc.*, **74** (1991) in press.
27. Cook, R. F. & Roach, D. H., The effect of lateral crack growth of contact flaws in brittle materials. *J. Mater. Res.*, **1**(4) (1986) 589–600.
28. Marshall, D. B. & Lawn, B. R., Residual stress effects in sharp contact cracking. *J. Mater. Sci.*, **14** (1979) 2001–12.
29. Lai, T. R., Hogg, C. L. & Swain, M. V., Comparison of fracture toughness determination of Y-TZP materials using various testing techniques. In *Ceramic Developments*, ed.

C. C. Sorrell & B. Ben-Nissan. Materials Science Forum Vols 34–36, Trans. Tech. Publications Ltd, Switzerland, 1988, pp. 1071–5.
30. Shen, R. S., Zelizko, V. & Swain, M. V., Critical stress intensity factor K_{Ic} and elastic modulus measurement at elevated temperatures on 3Y-TZP and alumina ceramics. In *Proc. 1990 Symp. of the Austr. Fract. Group*, Sydney, 1990, pp. 9–16.
31. Lutz, H. E. & Swain, M. V., The importance of the internal stress intensity factor as a measure for the prediction of the strength degrading influence of inclusions in glass and ceramics (to be published).
32. Lutz, H. E., Microstructure and properties of Al_2O_3 and ZrO_2 ceramics with spherical pressure zones (in German). PhD thesis, Technical University of Hamburg, Hamburg, FRG, 1989.